Non-imaging Characterization Assessment of Shedding Events from Derelict Satellites near Geosynchronous Orbit (GEO)

Thomas M. Kelecy[1]
Boeing LTS
Mark A. Skinner
Boeing Research & Technology

ABSTRACT

There is plausible speculation that retired satellites near geosynchronous orbit are the source of a debris population that was passively shed over time due to environmental effects. Recent initiatives intended to characterize these defunct satellites via analysis of non-imaging observations have established the ability to derive some of their physical and dynamic attributes. For long term observing of objects, what kinds of changes might one be able to detect that might be attributed to shedding? Are there any attributes common to both the shed piece of debris and the parent object that might allow one to tie the two together? The work presented attempts to shed some light on these questions by establishing several plausible shedding scenarios which include appropriate dynamics, shapes and materials, and uses appropriate bi-directional reflectance distribution functions and Long Wave Infrared (LWIR) models to create a simulated time history of observations that can be examined to analyze the shedding phenomenon. The goal of this work is to provide some insight into what characterization changes one might attribute to shedding when observing a "parent" object over an extended period. The results show that astrometric, photometric, albedo-area product, and multi-wavelength brightness observations each provide unique characterization attributes which, when combined, allow one to infer shedding phenomena.

1. MOTIVATION AND GOALS OF THE WORK

There is a known and well-tracked population of defunct satellites [1, 2] in the so-called "graveyard orbit" which is the post-mission disposal region for satellites in geosynchronous (GEO)[2] orbit located at altitudes several hundred kilometers above the geostationary altitude (~35786 km) [3]. These drifting, non-station-kept objects have a variety of ages and sizes, and exhibit behavior quite different from operational, station-kept satellites orbiting in GEO. In addition, new objects are now appearing in this volume of space in and around the geostationary arc and graveyard orbit. These objects may be pieces shed from other objects, or previously un-catalogued objects that have been detected as the result of better and more sensitive space surveillance monitoring.

In attempting to understand the environment in and around the GEO belt, studies of this class of space objects [4, 5] are important to pursue for space flight safety [6, 7], and new studies are taking advantage of every opportunity to do so with as many sensors, wavelengths, spatial, and spectral resolutions as are now available. A benefit of studies resulting in a better understanding the shedding process is that it would provide insight into the environmental factors that contribute to the debris hazard. Another benefit is that it can help to identify major sources of shedding and, hence, provide potential candidate objects for future debris removal should that technology become viable [8, 9]. The study and understanding of the material makeup of shed debris will provide guidance for satellite design modifications that could help to mitigate shedding from future satellites. Lastly, identifying potential shedding sources can help to establish tasking priorities for continued observations, as well as inform international decision-making on guidelines and best practices for the long-term sustainable use of outer space [10].

[1] Now a Senior Scientist with *Applied Defense Solutions (ADS).*

[2] In this work we refer to the geostationary *ring* as the altitude at which the orbital period exactly matches the rotation of the earth, with zero eccentricity and zero inclination, such that the object appears exactly fixed in the sky from an earth-based observer. The geosynchronous *belt* describes that volume of space where the orbital period is synchronous with the rotation period of the earth but the inclination and eccentricity are non-zero and, hence, the object appears to trace out a "figure eight" in the sky relative to an earth-based observer.

The goals of the work presented here are to take steps towards answering the following questions: What sort of changes might one look for in observational measurements that would allow one to infer a physical change might have occurred due to shedding? If one is observing debris, what characteristics might one look for that link it back to a parent object? Some additional background information on space debris is provided in the subsequent sections, including what shedding related attributes can be inferred from diverse observations. Examples of these are then presented using simulated measurements and modeling to demonstrate shedding characterization using a variety of analysis techniques appropriate to the observations. A summary of what can be gleaned from the shedding analysis concludes this paper.

2. BACKGROUND ON DEBRIS SHEDDING

The mid 1960's saw the dawn of the commercial GEO satellite telecommunications era, which has provided many benefits to mankind. However, "as a result of past activities in space, a massive amount of space debris – non-functional and uncontrolled objects – has been left in Earth orbit and this poses a serious challenge to the sustainability of outer space" [10]. The material in the GEO orbit can be characterized as active or inactive payloads, rocket bodies, debris, or similar. One source of larger debris threatening the GEO ring is the population of non-functioning payloads and upper stages that were placed there, but were not able to be disposed of into orbits higher than GEO (as is the current practice) upon their end of life. These objects are trapped in the two gravitational wells ("pinch points") that are caused by the gravitational anomalies (more specifically, the tesseral components of the spherical harmonic expansion of the earth gravitational model) of the Earth at the equator [11]. Objects that are trapped in one (or both) of the wells oscillate back and forth over some span of longitude, passing through the wells with some characteristic periodicity determined by their specific orbits. Fig. 1 [12] shows the deflection due to the gravitational anomalies relative to a "mean" orbit while Fig. 2 shows the population growth of objects near the western "pinch point". The objects thus trapped are primarily defunct payloads, including the first commercial GEO communications satellite, Intelsat-1 F1 ("Early Bird") [13]. Table 1, below, provides an example of near GEO defunct satellites along with their ground-tracks in Fig. 3.

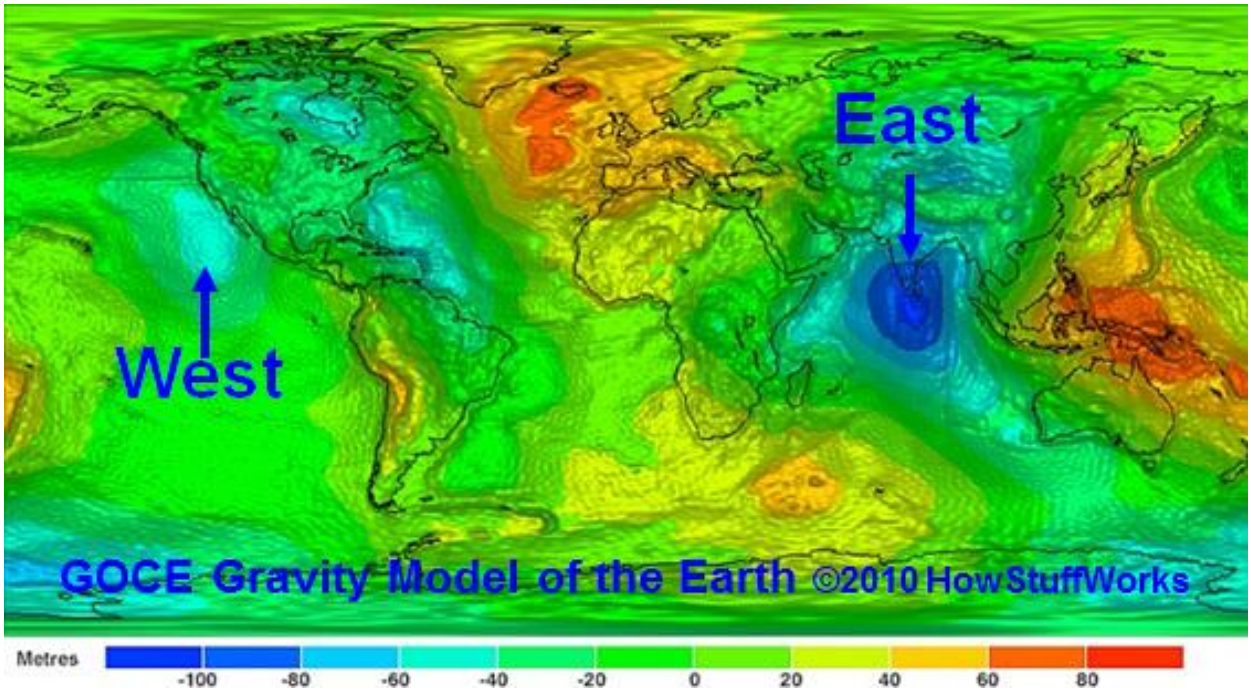

Fig. 1. Earth "West" and "East" Gravitational Anomalies (Pinch-points) – Deflection of Satellite Relative to Mean due to Gravity Anomalies [12]

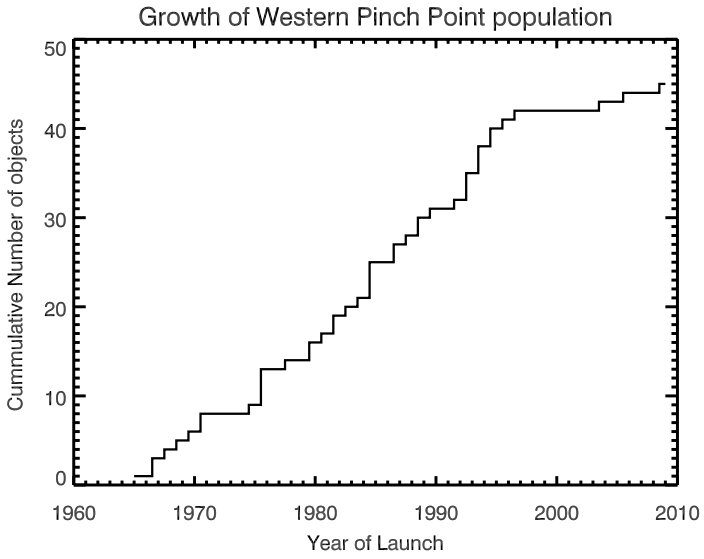

Fig. 2. Population History of Objects near the Western Pinch Point at 105° W. The change in slope of the curve ~1995 may be indicative of satellite operator compliance with GEO satellite end-of-life disposal guidelines.

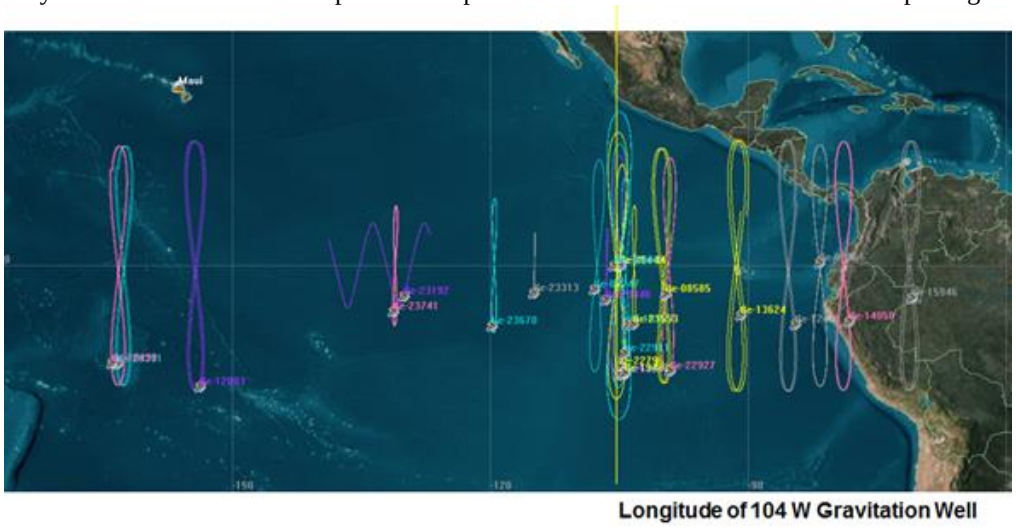

Fig. 3. Derelict Satellite Ground Tracks near Western Pinch Point

Table 1 List of Derelict Satellites near the Western Pinch Point

Name	Status	Year Inactive	Oscillation Period (years)	Oscillation Amplitude (deg)
GOES 1	Gravity well (close)	1985.0	2.5654	24.0
CTS	Gravity well (close)	1992.2	2.8282	40.0
LES 9	Gravity well (close)	2000.4	2.4641	5.5
RADUGA 7	Gravity well (far)	1987.0	3.9507	75.0
GOES 5	Gravity well (far)	1990.0	2.8501	38.5
GORIZONT 6	Gravity well (far)	1989.2	3.6468	71.0
SATCOM C5	Gravity well (close)	1997.0	0.4873	1.0
GOES 6	Gravity well (far)	1992.4	2.6420	30.0
GSTAR 1	Gravity well (close)	1997.0	0.4955	1.0
GSTAR 3	Gravity well (close)	1997.3	0.4901	1.0
COSMOS 2054	Gravity well (far)	1997.0	4.4271	80.0
RADUGA 25	Gravity well (far)	1998.0	3.6140	70.0
COSMOS 2209	Gravity well (far)	1997.0	4.1177	75.0
ACTS	Gravity well (close)	2001.0	0.5010	1.0
SOLIDARIDAD 1	Gravity well (close)	2000.9	2.4969	5.0
TELSTAR 401	Gravity well (close)	1997.0	2.5106	8.5
TELSTAR 4 (402R)	Gravity well (far)	2003.8	2.6174	16.5
GALAXY 3R	Gravity well (far)	2006.0	2.7122	30.0

The question arises of what happens to a piece of debris that is shed from a defunct satellite trapped in a pinch point? The stabilization is dominated by the gravitational anomaly, but there are other perturbations that affect the stability such as the Sun and Moon gravitation and solar radiation pressure (SRP). The amount of SRP acceleration imparted is a function of the cross-sectional area and mass of an object – the area-to-mass ratio (AMR) – and so if the shed component has a small AMR it will also remained trapped. However, if the shed piece of debris has a high AMR (HAMR), then that debris is "ejected" from the gravitational well and the perturbations will cause the orbit to migrate over long periods of time. As an example, Fig. 4 depicts a HAMR object having an AMR of 10 m^2/kg (vs. typical GEO satellite AMR of ~0.01-0.05 m^2/kg). It can be seen from the results that, after separating from a "stable" object location, the HAMR object becomes dislodged after around 18 years, primarily due to the higher SRP acceleration. More on this topic is presented in the next section.

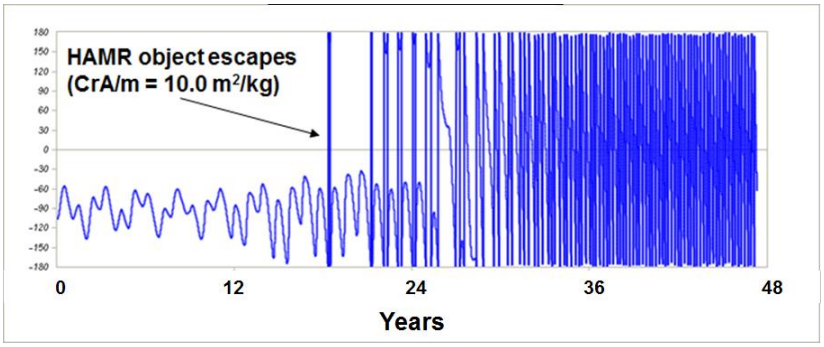

Fig. 4. High Area-to-mass Ratio Debris "Escaping" from Gravity Well

3. MATHEMATIC BASIS FOR MODELING OF OBSERVABLE SHEDDING PHENOMENA

3.1 Shedding Phenomena from Astrometric Observations

Astrometric observations provide "positional" metrics on the location and motion of an orbiting satellite. Models of the forces are used to determine and predict the motion based on the estimation of model parameters from the observational measurements. The force models for near-GEO satellites include the modeling of solar radiation pressure (SRP) forces which are a function of the size, orientation, mass and physical properties of the satellite surfaces. Fig. 5 is a notional depiction of these effects. The relevance for this discussion is that any change in size or mass, for example through shedding, will manifest itself in a change in orbit from what is predicted based on pre-shedding models.

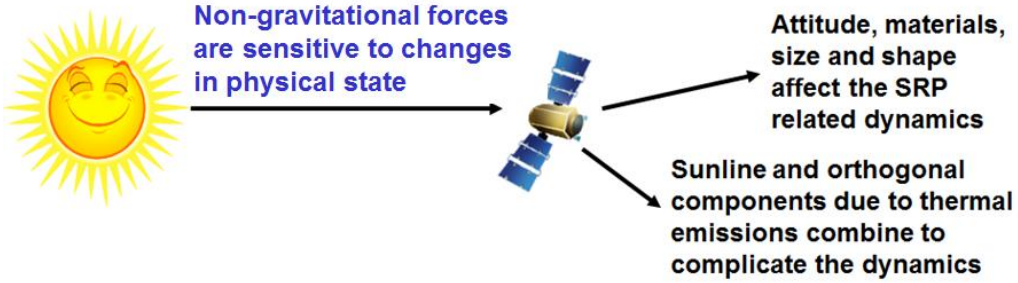

Fig. 5. Depiction of Solar Radiation Pressure Force Dependencies

The acceleration due to solar radiation pressure is computed as

$$\vec{a}_{SRP} = -\frac{1}{c}\sum_{i=1}^{NS}\frac{A_i}{m}\{F_P \Phi \vec{R}_i (\hat{k}_i \cdot \hat{n}_i) + \vec{P}_i\}$$

where the specular and diffuse terms are given by

$$\vec{R}_i = (1 - s_i)\,\hat{k}_i - \frac{2}{3} d_i\,\hat{n}_i + 2(\hat{k}_i \cdot \hat{n}_i)\,s_i\,\hat{n}_i$$

and the thermal emission related term is given by

$$\vec{P}_i = \frac{2}{3} a_i\,\sigma\,T_i^4\,\hat{n}_i$$

The various terms are defined as

c = *speed of light*

s_i = *specular reflectivity of surface i*

d_i = *diffuse reflectivity of surface i*

a_i = *absorption of surface i*

σ = *Stefan – Boltzmann const.*

T_i = *temperature of surface i in* deg *Kelvin*

$\hat{k}_i$ = *inertial unit direction of light incident on the surface*

$\hat{n}_i$ = *inertial unit surface normal of area* A_i

$(\hat{k}_i \cdot \hat{n}_i)$ = cos *of the angle between incident light and unit surface normal*

F_P = *incident solar flux*

Φ = *eclipse function*

NS = number of surfaces
Ai = effective cross-sectional area

The main thing to note from the equations modeling SRP acceleration is that the acceleration is a function of the size (area A) and mass (m) and so a significant change in either parameter will result in a perturbation to the orbit which deviates from the expected nominal. Hence, a significant shedding event will eventually be seen after some level of persistent tracking. The time it takes to manifest itself depends on the effective area to mass ratio (AMR = A/m) where larger changes in value will manifest themselves sooner than smaller changes.

Based on available information on their dimensions and masses, the AMR of a TDRS satellite can range from 0.0018-0.0316 m^2/kg and that for DirectTV-2 0.004-0.0456 m^2/kg [4, 5]. In contrast, if one of them should lose a sheet of multi-layer insulation (MLI), which has an AMR of about 20 m^2/kg, the orbit of the satellite and shed MLI will deviate significantly due to differing SRP accelerations since the pre-shedding orbit of the satellite would remain virtually unchanged due to the low mass loss. An in-depth analysis of sensitivity to modeling errors of the physical properties relevant to SRP (*e.g.* reflectivity, size, mass, inertia) is presented in [14].

3.2 Shedding Phenomena from Photometric and Albedo Area Product Observations

The bidirectional reflectance distribution functions (BRDFs) used to model photometric measurements are a function of various physical properties of the modeled satellite and the orientation of its surfaces with respect to the sun and observer [15, 16]. Shedding events can be detected in photometric and LWIR observations by virtue of the changes in attitude, size (cross-sectional area) and reflective and emissive properties. For the analysis to be presented, an "intact" model of a GEO satellite can be modeled as consisting of components each of which is made up of a subset of defined "facets." An example of a TDRS-10 "wire-frame" model is shown in Fig. 6 where the components consist of a bus, two solar wings and two "single axis" antennas.

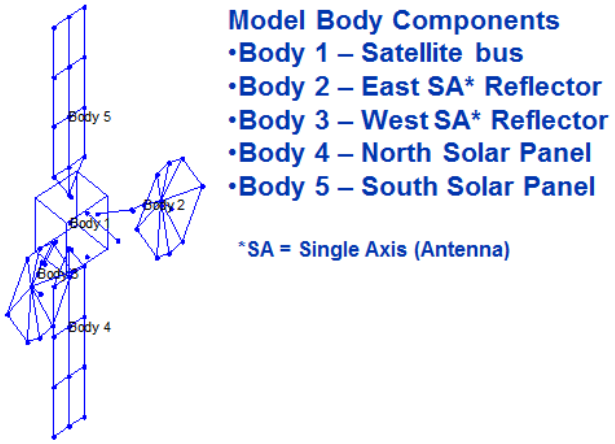

Fig. 6. Wire Frame Model of TDRS-10

The physical characteristics that are relevant to the modeling of a satellite include its size, mass and optical properties. Typical values for a (defunct) GEO satellite are provided in Table 2; these are used in the subsequent attitude dynamics and photometric modeling and analysis of shedding events.

The attitude dynamics equations of motion are presented in terms of the 3-axis body rates ω as [17]

$$\frac{d\boldsymbol{\omega}}{dt} = \boldsymbol{I}^{-1}[\boldsymbol{N} - \boldsymbol{\omega} \times (\boldsymbol{I}\boldsymbol{\omega})]$$

where

$$\boldsymbol{I} = \boldsymbol{body\ moment\ of\ inertia\ matrix}$$
$$\boldsymbol{\omega} = \boldsymbol{body\ rate\ vector}$$
$$t = \boldsymbol{time}$$
$$\boldsymbol{N} = \boldsymbol{torque\ vector}$$

It should be noted that the moment of inertial matrix (I) is a key mass property dictating attitude dynamics and that, in the case of a significant shedding event, will result in a notable change in body rates and attitude of an uncontrolled defunct satellite. In general a separation will result in a reduction of the moment of inertia and change in the center of mass which ultimately increases the body rate of the main body.

Table 2. Representative Physical Properties of Typical GEO Satellites

Object	Comments	Length (m)	Width (m)	Height (m)	Area (m^2)	Mass	CrA/m (m^2/kg)	Material	Diffuse	Specular	Spec Idx	Albedo
Bus												
Case #1	TDRS like properties	1.7889	1.7889	1.7889	3.20	888.00	0.0036	Mylar	0.6	0.4	10	1.0
Case #2	DirecTV properties	2.3452	2.3452	2.3452	5.50	1134.00	0.0049	Mylar	0.6	0.4	10	1.0
Solar panel(s)												
Case #1	Single segment	2.5400	2.1590	0.0500	5.50	14.00	0.3929	Solar cell	0.4	0.6	200	1.0
Case #2	Whole 4-segment array	10.1600	2.1590	0.0500	21.94	56.57	0.3878	Solar cell	0.4	0.6	200	1.0
MLI sheet												
Case #1	Larger MLI sheet	1.0000	1.0000	0.0010	1.00	0.05	20.0000	MLI	0.9	0.1	3	1.0
Case #2	Smaller MLI sheet	0.5000	0.5000	0.0010	0.25	0.01	20.0000	MLI	0.9	0.1	3	1.0
Strut/yoke												
Case #1	Attaches SP to bus	0.6471	0.6471	0.0500	0.43	14.42	0.0299	Copper	0.8	0.2	2	1.0
Case #2	Attaches SP to bus	0.6571	0.6471	0.0500	0.53	14.42	0.0368	Copper	0.8	0.2	2	1.0
Booster												
Case #1	Small aluminum stage	7.0000	3.0000	3.0000	21.00	2720.00	0.0077	Aluminum	0.5	0.5	10	1.0
Case #2	Centaur upper stage	13.0000	3.0000	3.0000	39.00	2247.00	0.0174	White paint	0.9	0.1	200	1.0
Honeycomb												
Case #1	Generic panel segment	1.0000	1.0000	0.1000	1.00	91.00	0.0110	Aluminum	0.5	0.5	5	1.0
Case #2	Generic panel segment	1.0000	1.0000	0.1000	1.00	16.00	0.0625	Aluminum	0.5	0.5	5	1.0
Antenna dish												
Case #1	Gold plated mesh molybdenum	3.0000	3.0000	0.2000	9.00	10.00	0.9000	Gold	0.2	0.8	200	1.0
Case #2	Little dish antenna	2.1213	2.1213	0.2000	4.50	5.00	0.9000	White paint	0.9	0.1	200	1.0

3.3 Shedding Phenomena from Multi-band Brightness Observations

The modeling and estimation of physical surface properties of a "wire-frame" satellite were derived and presented in detail in by Hall et al. in [18, 19]. The optical cross section (OCS) is modeled as a function of facet sizes, shapes, orientation, and wavelength as

$$OCS(t,\lambda) = \sum_{j,m} f_{j,m}\, K_{j,m}(t,\lambda) \qquad \text{Optical Cross Section } [\text{m}^2\ \text{ster}^{-1}]$$

$$j = 1 \ldots N_{\text{Components}} \qquad \text{Satellite components}$$
$$m = 1 \ldots N_{\text{Materials}} \qquad \text{Candidate surface materials}$$

$$f_{j,m} = \text{Fraction of component } j \text{ covered with material } m$$
$$0 \le f_{j,m} \le 1 \quad \& \quad \left[\sum_{m} f_{j,m} \right] = 1$$

$$K_{j,m}(t,\lambda) = \text{Kernel depends on shape/orientation of satellite component } j \text{ and BRDF of material } m$$

The approach selected for use in subsequent analysis uses a catalog of materials properties [20] and the Bi-directional Reflectance Distribution Function (BRDF) uses the Maxwell-Beard formulation for modeling the diffuse and specular reflection properties of specific materials as a function of sun-observer illumination angles and the wavelength of the observing sensor [21, 22]. The concept is applied to show that if a defunct satellite's material properties can be characterized *a priori*, then if a component or material is shed, this change can be detected from subsequent multi-wavelength observations. This would provide a means for detecting shedding if the mass properties do not change significantly, *i.e.* the property change is not sufficiently large to case a perturbation in the orbit and/or attitude dynamics. An example implementation and results are presented in the next section.

4. CHARACTERIZATION OF SHEDDING FROM OBSERVATIONS

4.1 Characterization of Shedding from Astrometric Observations

Several scenarios were run where various satellite components were propagated over a 50-year span using analytical equations which account for the mean effects of Earth, Sun and Moon gravitation, and solar radiation pressure. This Long-term Orbit Propagation (LOP) was run on an intact satellite, a solar panel, the satellite bus only, a dish antenna, and a sheet of multi-layer insulation (MLI). The key AMR properties are provided in Table 2. The goal of this exercise is to compare the key orbital parameters, such as semi-major axis (sma), eccentricity (ecc), and inclination (inc), between the component orbits to gauge how they separate as a function of time as an indirect measure of change due to shedding.

One might be able to detect shedding via the long-term tracking and orbit determination and AMR values for the tracked objects. If there is a shedding event that results in a significant enough change in the AMR, that change would be noted by deviations of the orbit relative to the pre-shedding AMR and potentially a modified estimate of the AMR value. Accurate tracking measurements and modeling fidelity are required to obtain accurate AMR estimates, and even then, the AMR values will likely vary over time as the result of the uncontrolled attitude of the debris objects and/or defunct satellite.

The values of semi-major axis and eccentricity change very little over the 50 year time span for an intact satellite having an AMR of around 0.05 m^2/kg. As expected, the inclination grows to a maximum of around 15° over a 50 year cycle due to lunar-solar effects. The AMR value of a separate solar panel is about 0.4 m^2/kg and does change

relative to the intact satellite as shown in Fig. 7, but the change is only noticeable after around 25 years. The thermal SRP effects were not modeled in this case and so could result in larger deviations over a given time span [14].

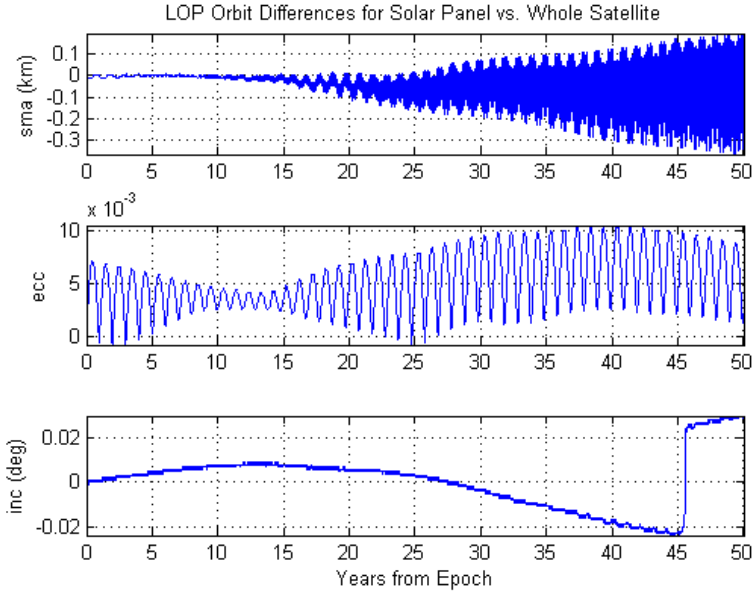

Fig. 7. Long-term Orbit Propagation (50 years) Orbit Differences: Solar Panel vs. Whole Satellite

However, in the case of a sheet of MLI having an AMR value of around 20 m^2/kg, the change in orbital elements relative to the intact satellite orbit happens fairly quickly and it only takes a few months to see the changes. The relative orbit change history for semi-major axis, eccentricity and inclination are shown in Fig. 8.

The result is that using astrometry to track and estimate the orbit and AMR values can be used to observe shedding events via changes in AMR, however, the changes happen only slowly and so the determination of shedding is evident only after tracking over a span of years to "see" the deviation from pre-separation predictions.

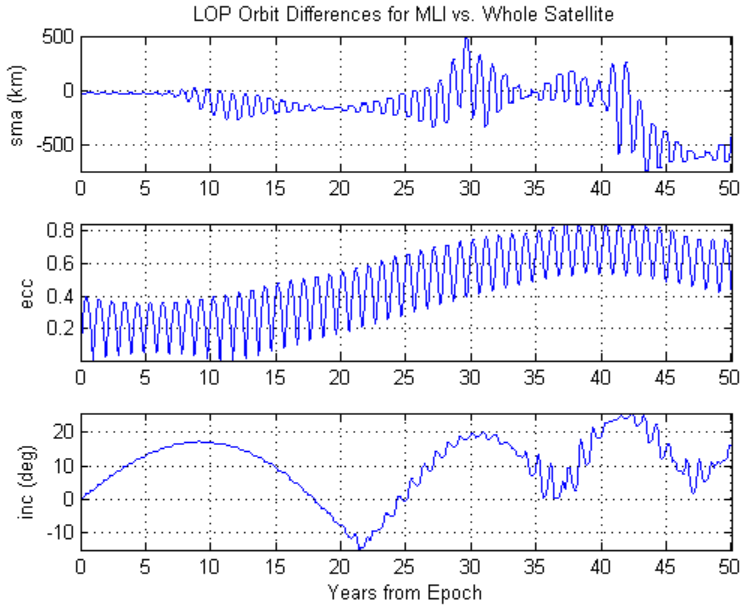

Fig. 8. Long-term Orbit Propagation (50 years) Orbit Differences: MLI vs. Whole Satellite

4.2 Characterization of Shedding from Photometric and Albedo Area Product Observations

The derivation of shape and attitude from photometric signatures has been developed and demonstrated over the past several years [15, 16]. A wire-frame model of DirecTV-2 mentioned previously in this paper was used along with albedo-area product (aArea) and photometric visual magnitude measurement (M_v) models from a sensor located at the Advanced Electro Optical System (AEOS) 3.67 m telescope on Haleakala, Maui. The satellite was assumed to be in an uncontrolled steady-state tumble as might be expected for an uncontrolled defunct satellite. The aArea and M_v time histories over a 10 minute interval are shown in Fig. 9 where the "tumble" signature is most evident in M_v, and the larger changes in area resulting from the full extent of the two solar arrays are reflected in the aArea history.

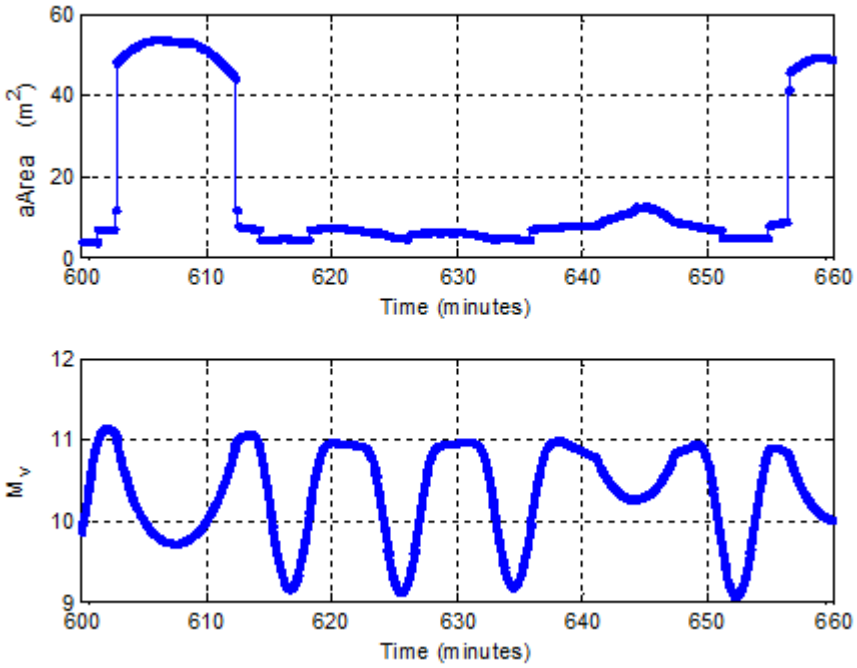

Fig. 9. Pre Solar Panel Shedding Photometric Signature for Tumbling Satellite

If we now assume that, between observations, a solar panel is shed, the change in the dynamic state will be reflected by a change in the size, *i.e.* a change in maximum total area, and also an increase in the rotation rate due to the change in moment of inertia due to the loss of the panel. The "post shedding" aArea and M_v history are shown in Fig. 10. It is evident that the maximum exposed area derived by aArea is reduced from around 50 m^2 to 30 m^2 for a similar observing geometry. This difference is approximately the size of a single solar panel. The M_v history does not change substantially, though the reduced rotation period (increased rotation rate) is easily evident as indicated as change in attitude dynamics due to the loss of the panel.

The conclusion is that significant changes in mass and size properties due to a shedding event can be observed through aArea and M_v observations. But what if the shedding does not result in a large-scale change in mass or size? This might occur, for example, as the result of a loss of a sheet of MLI covering a bus component. This case was run on a 3-axis stabilized GEO satellite. The loss of a ~4 m^2 sheet of MLI is not really observable in the aArea and Mv measurements as shown in Fig. 11 (same for pre and post shedding). However, if the removal of the MLI results in a significant change in the resulting albedo of the satellite, then although the area does not change, the albedo-area product can change enough to be detectable. Similarly, if one is conducting the monitoring observations in the LWIR, removal of an engineered thermal surface such as MLI might expose components with a much different value of emissivity, resulting in a similar change to the emissivity-area product.

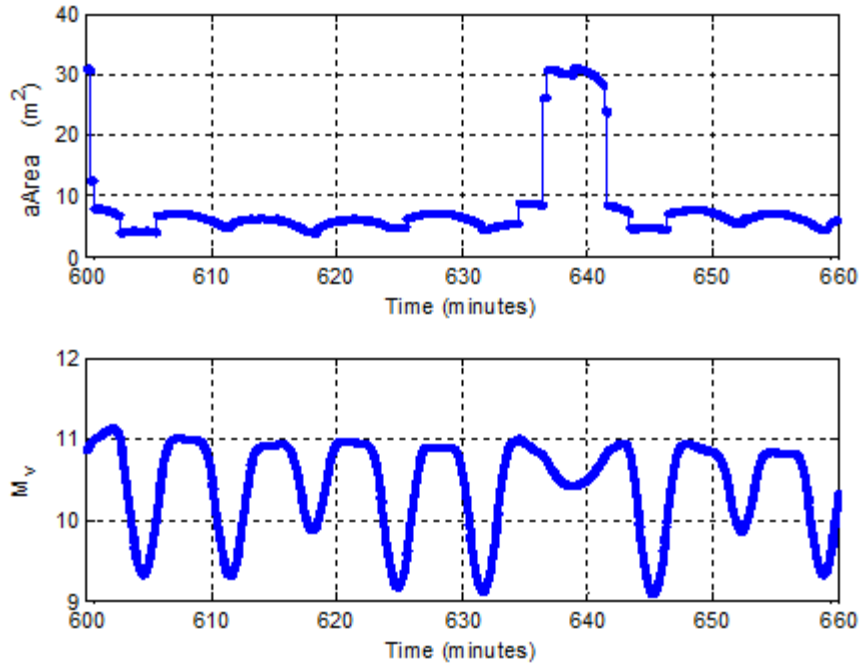

Fig. 10. Pre Solar Panel Shedding Photometric Signature for Tumbling Satellite

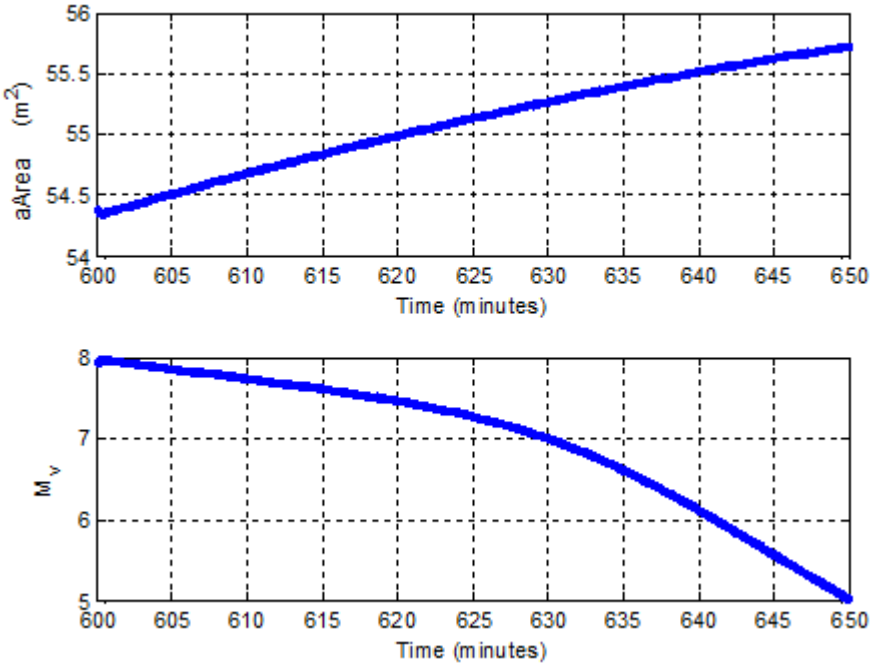

Fig. 11. Pre (and Post) MLI Shedding Photometric Signature for Stable Satellite

4.3 Characterization of Shedding from Multi-band Brightness Observations

The previous examples showed that astrometry and photometry can detect evidence of shedding, but have limitations depending on the size, mass and material optical properties changes involved in the shedding event. Although still being developed, the multi-wavelength brightness determination technique [18, 19] shows promise for

detecting separation events that do not involve large mass and/or size changes. It does require changes to the surface materials occur (e. g. due to shedding), the availability of a "wire-frame" model of the object being observed – including size, shape and attitude – in addition to a catalog of known materials properties. In this technique, one assumes that the material being observed is in the catalog. Yet another limitation is that if a surface is not observed using a multi-wavelength sensor, the surface material makeup cannot be determined.

As scenario was run where the modeled satellite was a cube (CUBESAT) of 2.5 m on a side. Before shedding the CUBESAT has solar arrays on the ±x and ±y surfaces, and insulation on the ±z surfaces. The CUBESAT is initially observed for 10 minutes per day over a 4 day period from the AEOS telescope where the satellite is spinning uniformly about the z-axis at 1° per second. The configuration and the derived photometric signature for 10 minutes of observing are shown in Fig. 12. Only slight variations in brightness are seen due to the rotation about the z-axis. The CUBESAT depicted in Fig. 12 is representative of the viewing aspect as seen by AEOS.

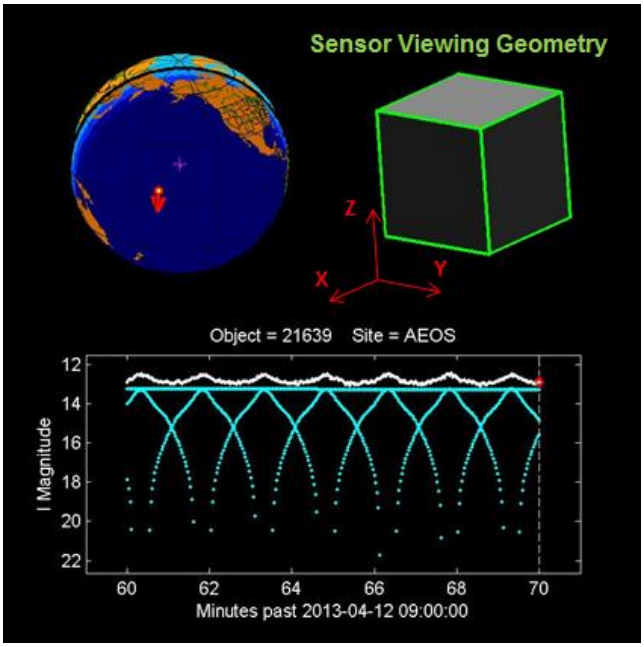

Fig. 12. CUBESAT Photometric Brightness History and Viewing Geometry

The multi-wavelength measurements produce a sequence of observations over a range of wavelengths as a function of time where this pattern will be uniquely determined by the surfaces and surface materials that are observed. An example of the pre-shedding CUBESAT materials is depicted in Fig. 13 with measurements as a function of wavelength and time are presented in Fig. 14.

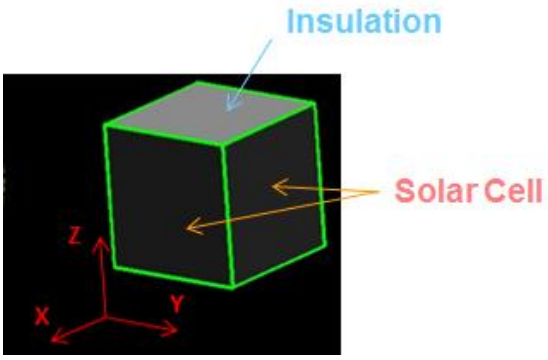

Fig. 13. Original CUBESAT Material Composition

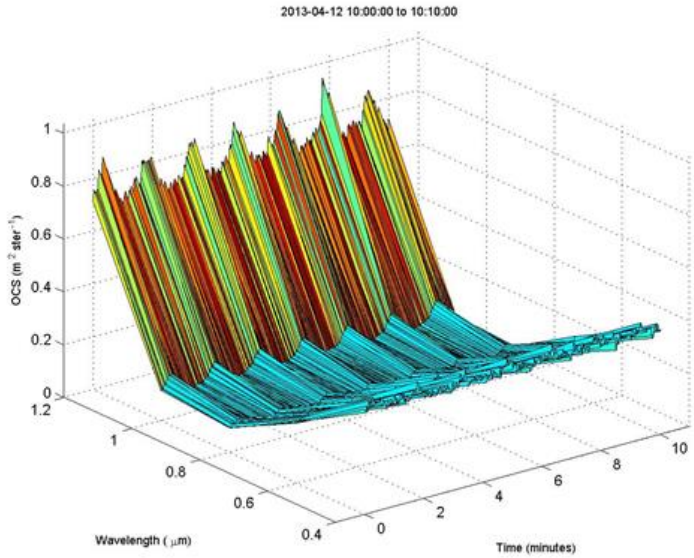

Fig. 14. Multi-wavelength Optical Cross Section vs. Wavelength vs. Time

The Material Abundance Estimation (MAE) method described in [18, 19] was applied where a catalog of 12 candidate materials was used to determine the best fit for all observable surfaces of the spinning CUBESAT. In this first case representing the pre-shedding configuration, multi-wavelength data were collected over a 1-hour observing span over each of 4 days and processed to estimate the surface materials. The results are shown in Fig. 15, which shows a matrix graphic of the 6 surface areas of the cube vs. the 12 candidate materials. The color scale shown on the far right goes from 0-1 (blue-red) to indicate the probability of a surface being made of a particular material. One can see that the MAE method correctly picked the solar panel material for ±x and ±y and the insulation material for +z. The –z surface was not observable due to the sensor-satellite geometry, so consequently that row is shown in black.

It was then assumed that the CUBESAT lost a complete panel from the +x surface to reveal an aluminum surface, and subsequently, a loss of the insulation on the +z surface to reveal a steel surface. Four 1-hour observations (over 4 days) were simulated after the shedding of the +x surface solar panel material and, again, the MAE correctly selected the new surface as being aluminum. Finally, another set of 1-hour multi-wavelength observations was generated over 4 days for the case where both +x and +z surfaces had shed material (Fig. 16) and the MAE method was again applied. The resulting solution matrix is shown in Fig. 17, where the correct solar panel materials are estimated for the –x and ±y surfaces while the +x is correctly determined to consist of aluminum and the +z correctly determined to consist of steel. Changes due to shedding are easily detected given the assumptions.

These idealized scenarios demonstrate that, at least conceptually, it might be possible to determine if shedding has occurred from an object if one could know the configuration and attitude of the satellite being observed, as well as assuming the correct materials are included in the catalog of candidate materials. Clearly, more work needs to be done to make this approach practical and feasible. One other detail in the implementation that needs to be consider is that of how one knows how to partition the data in a way that insures one applies the MAE method to a fixed configuration of surface materials? The answer is that one would have to potentially work through a combination of days of data to process in order to figure out an unambiguous solution. What if one were to process all 12 days of data which encompass the cases where 4 days represent the baseline configuration, 4 days represent the loss of the +x surface material, and the final 4 days represent both the loss of +x and +z surface materials? This combined configuration case was run and the results are provided in Fig. 18 where it can be seen that the estimation results in a more ambiguous set of solutions, though it still determines with a high likelihood the correct material composition of the –x and ±y surfaces, and hints at the correct +x and +z surfaces. The important conclusion being is that if one had previously characterized the pre-shedding materials as represented in Fig. 15, and subsequent measurements

produced solutions as shown in Fig. 18, one could confidently conclude that there was a change in the material composition of certain surfaces that might have been the result of shedding.

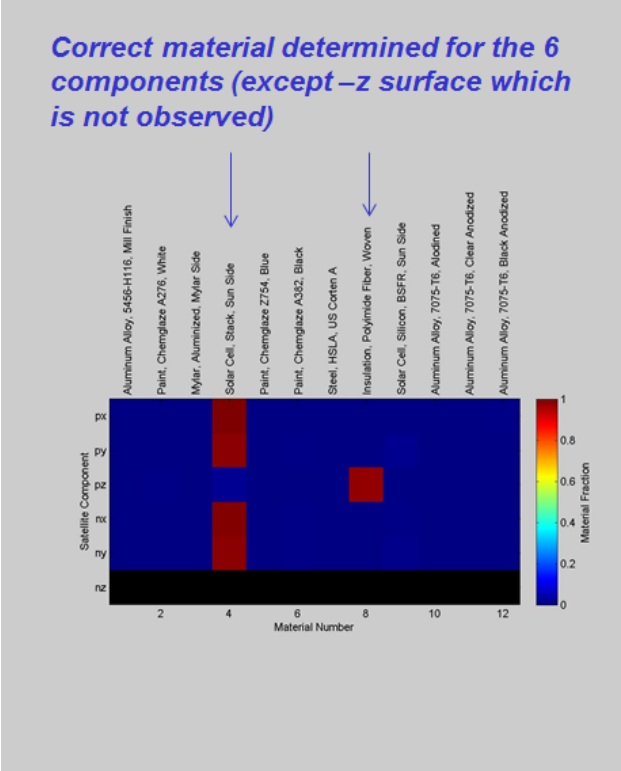

Fig. 15. Original CUBESAT Material Composition Estimated from Multi-wavelength OCS – 4 days x 1 hour

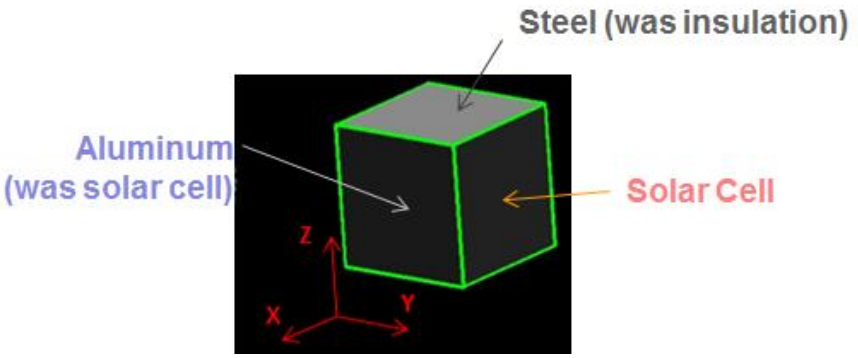

Fig. 16. Original CUBESAT Material Composition after Shedding Solar Panel and Insulation

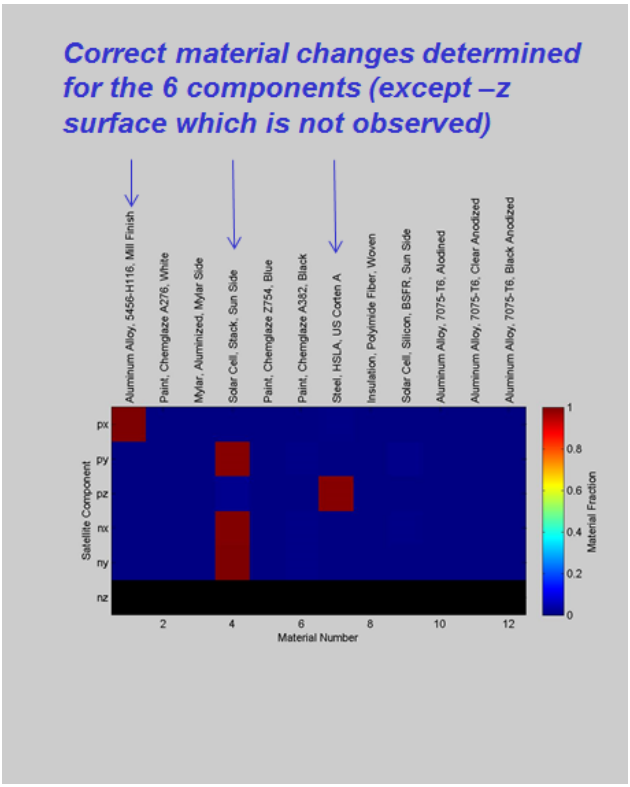

Fig. 17. Post Shedding CUBESAT Material Composition Estimated from Multi-wavelength OCS – 4 days x 1 hour

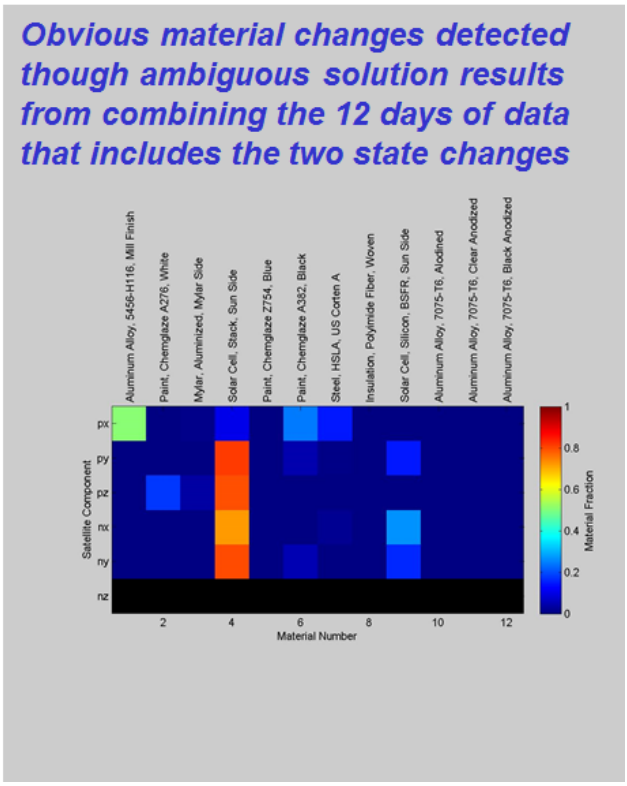

Fig. 18. Post Shedding CUBESAT Material Composition Estimated from Multi-wavelength OCS – 12 days x 1 hour

5. CONCLUSIONS AND RECOMMENDATIONS

The results of our modeling have shown that large-scale separations events (*e.g.* loss of a solar array) can be detected from astrometric observations over long time spans through long-term orbital parameter perturbations resulting from changes in the area-to-mass ratio. More immediate changes are observed in the photometric and albedo-area-product measurements through changes in effective area and changes to the attitude dynamics. Observations should be periodically conducted on derelict satellites and re-visit observations analyzed and compared to previous observations to detect potential state changes. The space catalog should also be searched for any "new" objects that are found subsequent to the detected changes and observations conducted on these new objects in an attempt to characterize their physical attributes to determine if they are consistent with a shed component.

Smaller scale separation events (*e.g.* loss of insulation material) are much harder to detect. Any use of astrometric data would require high fidelity orbit determination and prediction and the ability to predict back in time to determine if two objects were once connected to a single object. One potential approach was demonstrated where multi-wavelength brightness measurements might allow material composition measurements to be compared and examined for changes that might imply shedding. It is recommended that this technique be further developed and, in particular, a process developed which enables the shape and attitude information provided by the assumed known wire-frame model to be derived independently (*e.g.* from photometric data).

The origins of space debris at GEO are not definitively known, but the debris are suspected to be parts of derelict satellites launched in the past half-century. Our goal has been to determine how, from available observational and modeling methods, one could tell with high confidence if this is in fact the case. The results we might eventually reach could impact how we currently build satellites, and how we regulate the use of the space environment. To be able to achieve these insights, however, there must first be an intensive, long-term program of monitoring and characterization of these derelict objects.

6. ACKNOWLEDGMENTS

The authors would like to acknowledge Dr. Doyle Hall for his assistance in resurrecting some of the algorithms and models used for this analysis, and for his guidance and mentoring throughout our years of working together. We would also like to acknowledge Boeing's BR&T group, and in particular Dr. Paul Rodney, for funding support and advocacy for this work.

7. REFERENCES

1. R Choc, T Flohrer & B Bastida, *Classification of Geosynchronous Objects*, European Space Agency/European Space Operations Centre, Issue **13** (February 2011).
2. R Jehn, S Ariafar, T Schildknecht, R Musci, & M Oswald, "Estimating the number of debris in the geostationary ring" (2006) **59** Acta Astronautica 84.
3. *IADC Recommendation & Re-orbit Procedure for GEO Preservation*, Inter-Agency Space Debris Coordination Committee, IADC- 97-04, 1997.
4. Skinner, M., R. Russell, T. Kelecy, S. Gregory, R. Rudy. D. Kim and K. Crawford, "Observations in the thermal IR and visible of a retired satellite in the graveyard orbit, and comparisons to active satellites in GEO," 66th International Astronautical Congress, Jerusalem, Israel, October 2015.
5. Skinner, M., R. Russell, T. Kelecy, S. Gregory, R. Rudy. And D. Kim, "Comparison of Thermal IR and Visible Signatures of Graveyard Orbit Objects," Acta Astronautica 105 (2014) 1-10, 29 August 2014.
6. Mark Skinner, *Orbital Debris: What are the best near-term actions to take? A view from the field*, 2nd Manfred Lachs Intl. Conference on Global Space Governance, May 29-31, 2014, Montreal, Canada.
7. MA Skinner, *et al*, "*Hazards at GEO: The Space Debris population in the vicinity of the GEO belt and mitigation of its impact on commercial satellites*" (Address to the 30th AIAA International Communications Satellite Systems Conference (ICSSC), Ottawa, Canada, 24-17 September 2012).
8. D McKnight, "*Pay Me Now or Pay Me More Later: Start the Development of Active Orbital Debris Removal Now*" (Address to the AMOS Technical Conference, Wailea, Hawaii, September, 2010).

9. UNCOPUOS, *Active Debris Removal - An Essential Mechanism for Ensuring the Safety and Sustainability of Outer Space*, UN Doc A/AC.105/C.1/2012/CRP.16 (2012).
10. United Nations Office for Outer Space Affairs, COPOUS Scientific and Technical Subcommittee, 49th session, "Report of the Scientific and Technical Subcommittee on its forty-ninth session," A/AC.105/1001, Vienna, 6-17 February 2012.
11. Taylor, E.A., Orbit Theory and Applications, General Electric training material, http://www.cdeagle.com/, 1991.
12. Schiermeir, Q. "GOCE depicts gravity in high resolution," http://blogs.nature.com/news/2010/06/goce_depicts_gravity_in_high_r.html, 29 June 2010.
13. Abbot, Richard I. and Wallace, Timothy P., "Decision Support in Space Situational Awareness," Lincoln Laboratory Journal, Volume 16, Number 2, 2007, pp. 297-335.
14. Kelecy, T. and M. Jah, "Analysis of Orbit Prediction Sensitivity to Thermal Emissions Acceleration Modeling for High Area-to-mass Ratio (HAMR) Objects", *2009 AMOS Technical Conference*, Wailea, Maui, Hawaii, 1-4 September 2009.
15. Hall, D. "Separating Attitude and Shape Effects for Non-resolved Objects", The 2007 AMOS Technical Conference Proceedings, Kihei, HI, 2007
16. Kervin, P., Hall, D. and Bolden, M., "Phase Angle: What is it good for?" The 2010 AMOS Technical Conference Proceedings, Kihei, HI, 2010.
17. Wertz, J.R. (editor), "Spacecraft Attitude Determination and Control", Astrophysics and Space Sciences Library, Vol. 73., D. Reidel Publishing Co., Boston, MA, 1978.
18. Hall, D., "Surface Material Characterization from Multi-band Optical Observations", *2010 AMOS Technical Conference*, Wailea, Maui, Hawaii, 15-17 September 2010.
19. Hall, D., K. Hamada, T. Kelecy and P. Kervin, "Surface Material Characterization from Multi-band Optical Observations", *2012 AMOS Technical Conference*, Wailea, Maui, Hawaii, 11-14 September 2012.
20. Riker, J., and Butts, R., "The Time-Domain Analysis Simulation for Advanced Tracking (TASAT) Approaches to Compensated Imaging", SPIE Vol.1688, *Atmospheric Propagation and Remote Sensing*, 1992.
21. Cook, R.L and Torrance, K.E., "A Reflectance Model for Computer Graphics", *ACM Transactions on Graphics*, Vol.1, 7-24, 1982.
22. Torrance K.E. and Sparrow, E.M., "Theory for Off-Specular Reflection for Roughened Surfaces", *J. Opt. Soc. Am.*, Vol.57, 1105-1114, 1967.